

## Supplementary Materials

For

# High-Value Utilization of Silicon Cutting Waste and Excrementum Bombycis to Synthesize Silicon–Carbon Composites as Anode Materials for Li-Ion Batteries

Hengsong Ji <sup>1,†</sup>, Jun Li <sup>1,†</sup>, Sheng Li <sup>1</sup>, Yingxue Cui <sup>1,\*</sup>, Zhijin Liu <sup>1</sup>, Minggang Huang <sup>2</sup>, Chun Xu <sup>2</sup>, Guochun Li <sup>1</sup>, Yan Zhao <sup>3</sup> and Huaming Li <sup>1</sup>

<sup>1</sup> Institute for Energy Research, Jiangsu University, Zhenjiang 212013, China;

<sup>2</sup> Key Laboratory of Fine Chemical Application Technology of Luzhou, Luzhou 646099, China

<sup>3</sup> College of Chemistry and Chemical Engineering, Inner Mongolia University, Hohhot 010021, China

\* Correspondence: [yxcui@ujs.edu.cn](mailto:yxcui@ujs.edu.cn) (Y.C.)

† These authors contributed equally to this work.

## Supplementary Figures:

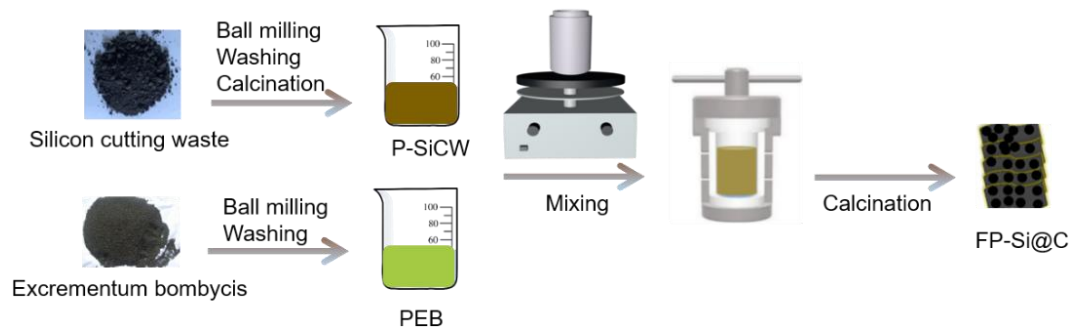


**Figure S1.** Schematic illustration of the synthesis process for FP-Si@C composites.

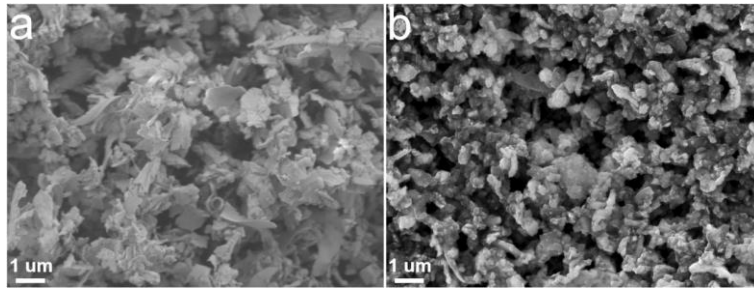


**Figure S2.** SEM images of (a) silicon cutting waste scragglomerations and (b) P-SiCW.

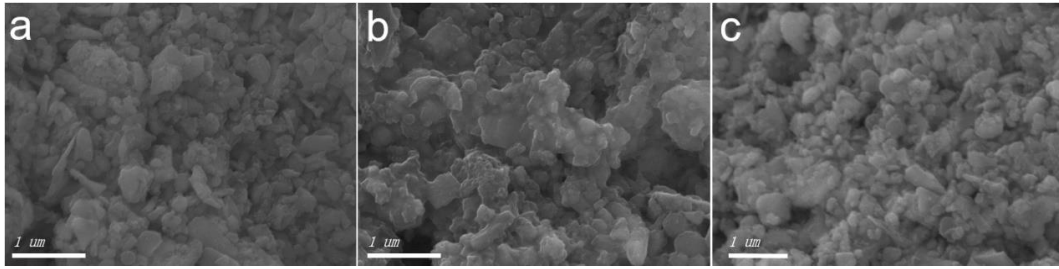


**Figure S3.** SEM images of (a) FP-Si@C-1, (b) FP-Si@C-2, and (c) FP-Si@C-3.

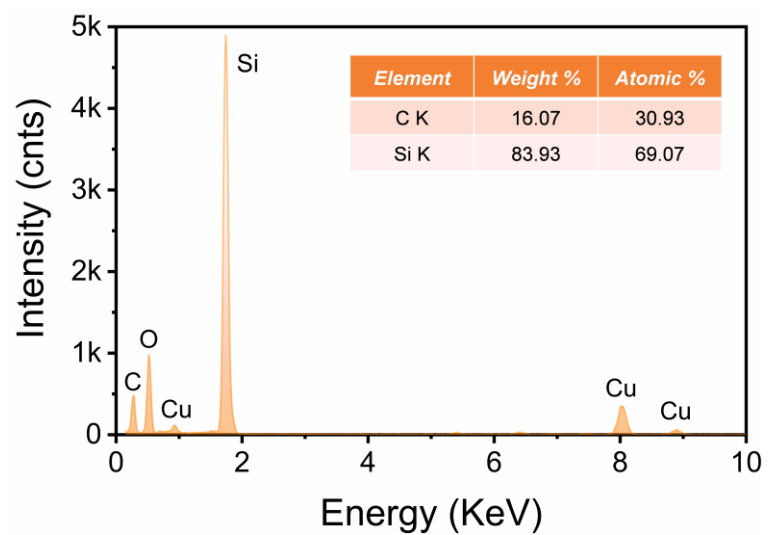


**Figure S4.** EDS spectrum of FP-Si@C-2 (Inset is the weight and atomic content of C and Si).

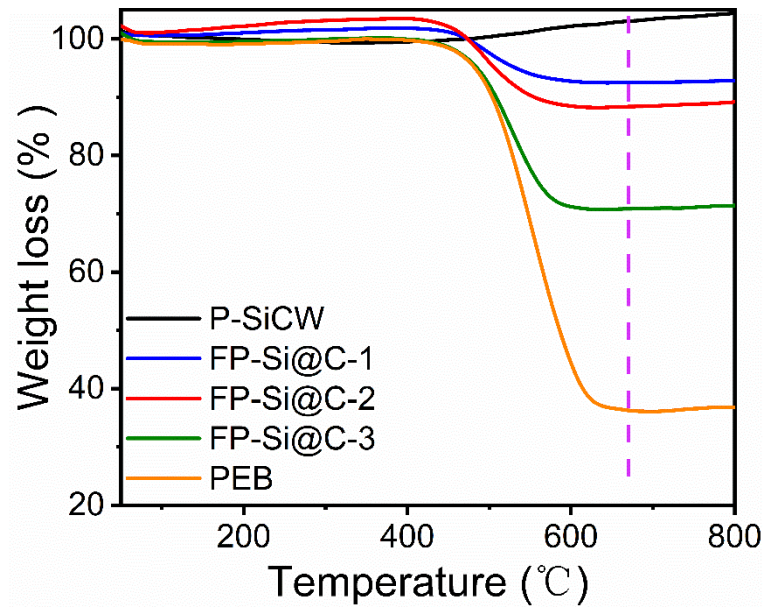
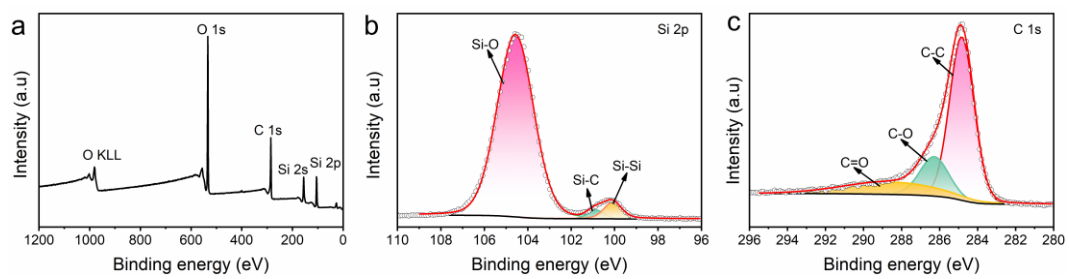


Figure S5. TGA curves of P-SiCW, PEB, FP-Si@C-1, FP-Si@C-2, and FP-Si@C-3.



**Figure S6.** (a) XPS full spectrum, (b) XPS Si 2p spectrum, and (c) XPS C 1s spectrum of FP-Si@C-2.

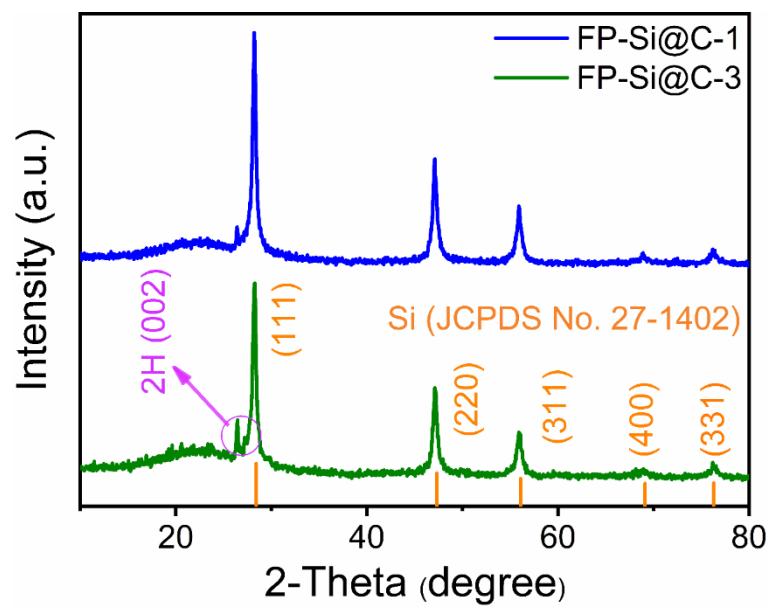
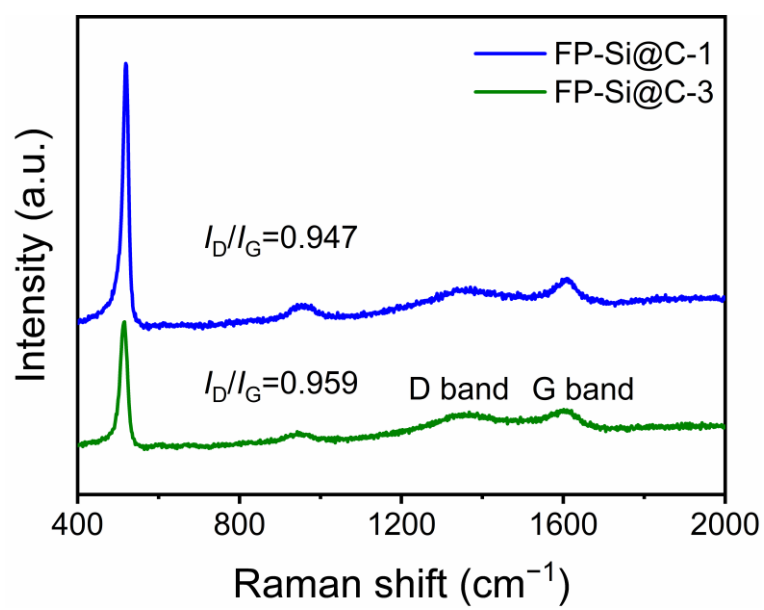
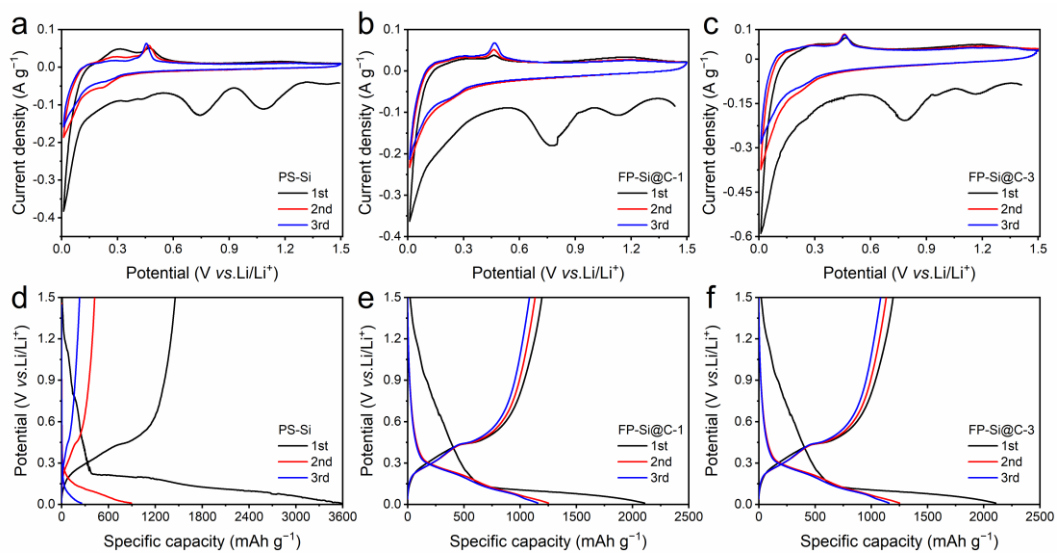


Figure S7. XRD patterns of FP-Si@C-1 and FP-Si@C-3.



**Figure S8.** Raman spectra of FP-Si@C-1 and FP-Si@C-3.



**Figure S9.** (a–c) The initial three CV curves of P-SiCW, FP-Si@C-1, and FP-Si@C-3 at  $0.1 \text{ mV s}^{-1}$ . (d–f) The initial three GCD curves of P-SiCW, FP-Si@C-1, and FP-Si@C-3 at  $0.1 \text{ A g}^{-1}$ .

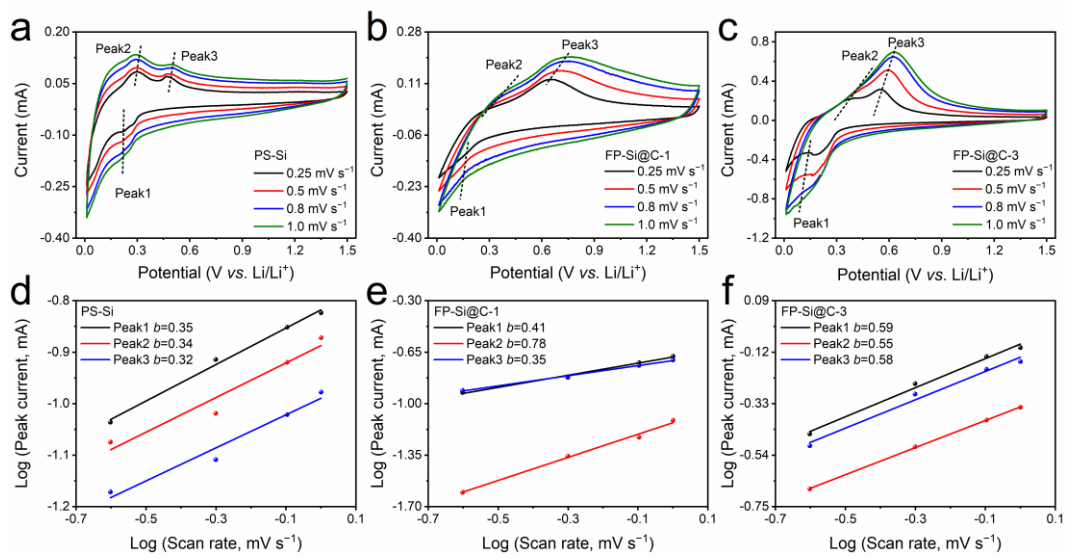


**Figure S10.** (a-c) The CV curves of P-SiCW, FP-Si@C-1, and FP-Si@C-3 at different scan rates. (d-f) The  $\log(i)$ - $\log(v)$  plots of P-SiCW, FP-Si@C-1, and FP-Si@C-3.

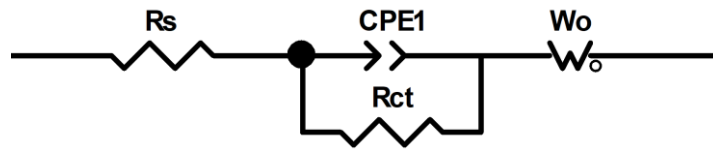


**Figure S11.** Equivalent circuit model linked with EIS curves.

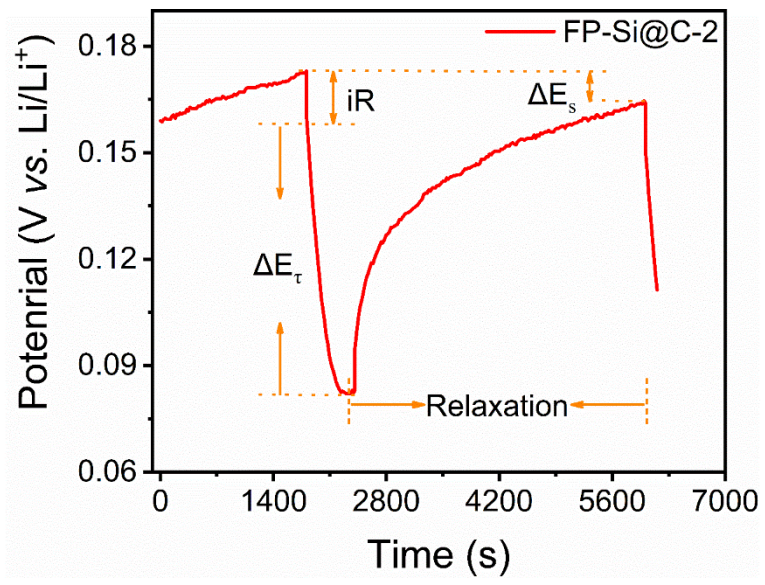


**Figure S12.** Partial enlarged view about GITT results and marked  $\Delta E_s$  and  $\Delta E_{\tau}$  of FP-Si@C-2.

**Supplementary Tables:**

**Table S1.** XRF results of silicon cutting waste and P-SiCW.

<b>Sample EA</b>	Si	Fe	Cr	Ni	Cu	Cl	Mg	Mo
Silicon								
<b>Weight</b> cutting (%) waste	83.84	10.34	3.44	1.8	0.134	0.0637	0.0382	0.037
P-SiCW	99.83	0.0067	0.0007	0.0256	0.0005	0.0027	0.0336	0.0043

**Table S2.** BET specific surface area, pore volume, and BJH pore size of P-SiCW and FP-Si@C-2.

<b>Sample</b>	<b>S<sub>BET</sub> (m<sup>2</sup> g<sup>-1</sup>)</b>	<b>V<sub>total</sub> (cm<sup>3</sup> g<sup>-1</sup>)</b>	<b>Average pore size (BJH) (nm)</b>
P-SiCW	113.50	0.24	8.31
FP-Si@C-2	61.76	0.14	9.32

**Table S3.** The  $R_{ct}$  and Warburg values of P-SiCW, FP-Si@C-1, FP-Si@C-2 and FP-Si@C-3.

<b>Sample</b>	<b><math>R_{ct}</math> (ohm)</b>	<b><math>\sigma</math> (<math>\Omega S^{-1/2}</math>)</b>
P-SiCW	97.8	46.9
FP-Si@C-1	102.8	27.2
FP-Si@C-2	91.5	25.9
FP-Si@C-3	116.5	40.2